SENSITIVITY OF VERTICAL AXIS WIND TURBINES TO ROTOR SHAPE AND BLADE DESIGN: A COMPUTATIONAL INVESTIGATION

N. Franchina[1], *O. Kouaissah*[1], *G. Barigozzi*[1], *G. Persico*[2,*]

[1]Dipartimento di Ingegneria e scienze applicate, Università degli Studi di Bergamo, Viale Marconi 5 - 24044 Dalmine (BG), Italy
[2]Dipartimento di Energia, Politecnico di Milano, via Lambruschini 4 - 20156, Milano
* Corresponding author, giacomo.persico@polimi.it

ABSTRACT

In this paper we present a computational investigation of the aerodynamics and performance of four vertical axis wind turbines, comparing two different troposkein rotors equipped with two different airfoil sections. Simulations were performed by resorting to an experimentally-validated 2D/3D unsteady Computational Fluid Dynamics model, based on the U-RANS formulation of the equation and relying upon the $k-\omega$ SST turbulence model in low-Reynolds formulation. The performance of the selected wind turbine configurations are investigated and discussed considering different operating conditions at 2D level, and then focusing on the peak efficiency condition for the fully 3D analysis. Overall power coefficient data and trends, spanwise distributions and local blade aerodynamics are used to discuss the impact of rotor solidity, Reynolds number, and airfoil shape on turbine performance. The investigation reveals that the adoption of non-symmetric laminar profiles provides important advantages in complex flow regions, typical of such class of machines, both in the equatorial sections and along the span. Moreover, a solidity formulation based on the equatorial section turns out to be representative of the aerodynamics of the entire turbine, despite the trospokein shape of the rotor.

KEYWORDS

VAWT blade design, VAWT experimental assessment, URANS modeling, 2D-3D VAWT performance prediction, Troposkein wind rotors

Nomenclature

c	blade chord $[m]$	D	turbine diameter $[m]$, drag $[N]$
k	turbulent kinetic energy $[m^2/s^2]$	L	lift $[N]$, blade length $[m]$
n	rotational speed $[rad/s]$	H	turbine span $[m]$
C_M	moment coefficient C_M=M/(1/2ρ_∞ V_∞^2 AR) $[-]$	M	moment $[Nm]$
		P	power $[W]$
C_P	power coefficient $C_P = C_M\, TSR$ $[-]$	R	turbine radius $[m]$
A	turbine frontal area $[m^2]$	URANS	Unsteady Reynolds Averaged Navier-Stokes

Re	Reynolds number $[-]$	α	incidence angle $[deg]$
SST	Shear Stress Transport	ω	vorticity $[1/s]$
TSR	Tip Speed Ratio	ρ	density $[Kg/m^3]$
Tu	turbulence intensity Tu= $\sqrt{2k/3}$/V$_\infty$ $[-]$	σ	solidity σ=NcL/A $[-]$
		θ	azimuthal angle $[deg]$
U	peripheral velocity $[m/s]$, uncertainty [-]	Δt	time step $[s]$
V	absolute velocity $[m/s]$	Δx	spatial discretization parameter $[m]$
VAWT	vertical-axis wind turbine	∞	freestream
W	relative velocity $[m/s]$	eq	equatorial

1 Introduction

Sustainable energy ambitious targets driven by severe climate changes have recently promoted a great demand for innovative solutions for exploiting renewable energy sources. Onshore and offshore wind turbines, possibly employed in wind farms, are a very promising choice and are expected to play a key role in the current, complex, energy scenario. As documented in the Global Wind Energy Council 2022 report, the total installed wind-turbine capacity amounts to 837 GW, a growth of 12.4% compared to 2020; in the next years, the wind energy role as a key player for the energy transition will depend on ensuring the industry's growth is sustainable, socially responsible, while relying upon a clear and viable economic perspective. In such a scenario, multiple wind turbine technologies need to be considered with the aim of selecting the most promising configurations for the specific application context.

Beside the mainstream horizontal-axis wind turbine, the lift-driven Darrieus vertical-axis wind turbine (VAWT) has received a growing attention in the last decades from both academic groups [22, 17, 34, 15, 23, 16, 7] and institutions [26, 27] for its peculiar characteristics [13]: i) a good candidate for installations in a network of local energy community (within complex turbulent flows developing in urban environment) and ii) a potential competitor for large-scale wind installations offshore, especially in connection to floating foundations. In particular, these machines are endowed of a low center of gravity, being the drive train and generator placed at the bottom of the tower, and thus not affected by cyclic gravitational loads that may cause fatigue damages. However, the rotor operation gives rise to unsteady, cyclic variation of the load experienced by the blades and overall structure; moreover, the flow field establishing is inherently unsteady and fully three dimensional, transitional to turbulent, and often featuring local separations on the blades, greatly complicating the investigation of the turbine operation and performance.

Accurate prediction of the aerodynamic performance of VAWTs is clearly of great relevance to obtain innovative solutions both for small-scale distributed applications and for utility-scale installations in large wind farms. Recent works have enriched the experimental database on prototypes at laboratory scale [22, 17, 34, 15, 23, 16, 7], have proposed or improved tailored modeling techniques for aerodynamic predictions, also considering multiple fidelity level [32, 2, 3, 4, 11, 28, 8, 20, 5], and have investigated issues related to the machine operation [10, 31, 25, 21].

High resolution CFD simulations can help to gain deep insight into flow structure development, and better understanding of the energy harvesting process. In fact, several issues play a key role in the optimization of the power exchanged: i) the machine geometry, in particular the blade section (due its effect on the power harvesting at different TSR conditions as shown in [35], where a morphing design of airfoils was adopted to obtain the optimal airfoil shape at lower TSR values), the turbine solidity (see for example, [24], in which two different solidity configurations are studied for a selected base geometry, by varying the number of blades), and the rotor aspect ratio; ii) the operating parameters such as the TSR value, the flow regime, the turbulence intensity level (as presented in [33]), or such as the Reynolds number (see for example [30], where the effects of a blade profile, the Reynolds number, and the solidity on VAWT performance were investigated using a multiple stream tube method); iii) viscous losses as for example those due to the presence of the shaft (see *e.g.* [29] where a quantification of power losses is provided for a urban scale VAWT using 2D CFD computations). Several issues are relevant for the effective design of VAWTs, also owing to the combined effect of those key issues, and therefore further investigations are certainly needed to extend the field of knowledge with respect to these topics, in order to improve the performance of existing configurations and to conceive innovative, more performing machine configurations.

The rationale behind this work consists in providing a further step forward in the analysis of VAWTs behaviour, by applying a high-resolution computational model, endowed of proper experimental validation. The considered turbine rotor is characterized by a Troposkein shape and two different airfoil profiles are selected. The Troposkein configuration was selected since, during recent years, it received renewed attention for its technical advantages, which may promote its application in offshore wind farms, with water depths greater than 40 meters (see for instance [36, 6, 9]). The selected rotor is then assessed considering a symmetric profile and a cambered one. In this paper we first document a wide 2D computational campaign, aimed at investigating the influence of the solidity parameter at different machine operating conditions when applied to several different configurations, *i.e.*, different rotor sizing, blade shaping and airfoil design. Then, fully-3D calculations of the flow field around selected rotor configurations is also presented to investigate the performance prediction at relevant operating conditions, so to derive engineering-relevant conclusion on key design parameters.

2 Turbine Models and methodology

Different configurations of laboratory-scale wind turbine models are considered to study the influence of geometrical and operating parameters on the machine capability of power exchange. The selected configurations, shown in Figure 1 are as follows:

1) A rotor designed with a troposkein architecture, named TW, a 1-kW class machine, which can be regarded as either a real-scale turbine for distributed micro-generation within energy communities or as a small-scale laboratory model of a utility-scale device, *e.g.* for off-shore floating wind farms. Full details on the rotor geometry (including the tabulated coordinates of the troposkein profile) and the experimental results (including tabulated data) are reported in [7].

2) The Deepwind troposkein wind tunnel model herein called DW is studied in [6], where full details on the rotor geometry (including the tabulated coordinates of the troposkein profile) and the experimental results are provided.

Table 1 lists the main relevant, geometrical data of the turbine rotors selected as above described. These models have been chosen since their original design was tightly related to the DeepWind turbine featuring Troposkein blade shapes; specifically, assuming to fulfill a good

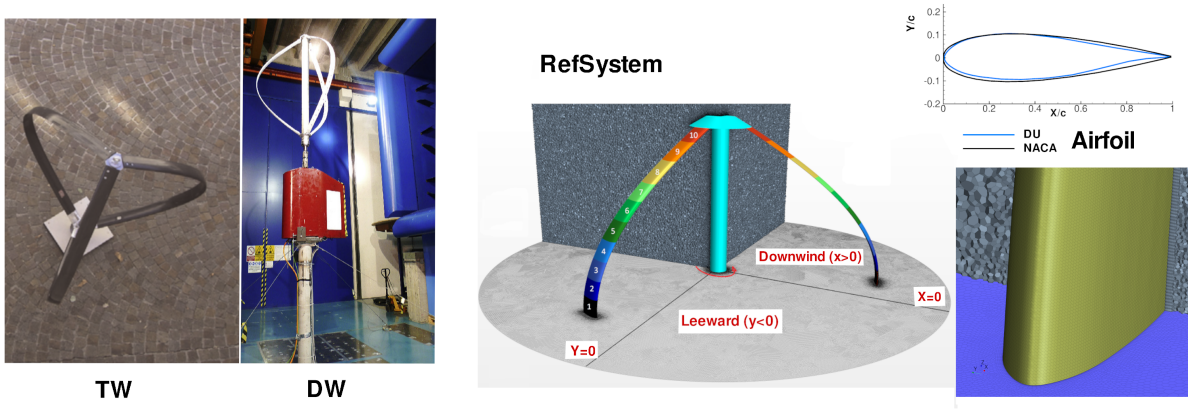

Figure 1: TW & DW Rotor models (left); VAWTs reference system and selected airfoil profiles, blade profile $f(z)$ with slices from midspan to top, 1 to 10 (right)

mechanical resistance, the machine performance is tightly related to the airfoil profile, and to geometrical features connected to the swept area and to the blockage effects. Furthermore, a symmetrical NACA profile is then compared with the DU06W200 profile (developed by [12]) specifically designed to obtain enhanced aerodynamic performance, in order to set a quantitative comparison in between different design approaches. Indeed the research activity on the rotor aerodynamics and performance behaviour of a troposkien VAWT still remains a challenge due to complex evolution within the structure and behind it.

VAWT	Rotor	Airfoil	h_b [m]	D_r [m]	A [m^2]	σ	Re_u
TW	Troposkein	NACA0021	1.510	1.510	1.5	0.054	190k
DW	Troposkein	DU-W06 W 200	1.902	2.028	2.63	0.047	220k

Table 1: Model VAWTs test cases: main geometrical parameters

Figure 1 allows to drawn a first comparison between the different profiles. Notice that only the models reported in Table 1 were actually investigated experimentally in the large-scale wind tunnel of the Politecnico di Milano; these were performed in free-jet configuration, with jet cross-section 4×3.8 m^2 (sufficiently large to make negligible the free-jet blockage). Full details on the measurement techniques and on the wind tunnel and achieved results are reported in [7, 6].

3 Numerical methodology

URANS computations documented in this paper were carried out using the Starccm+ multi-physics code [1]. The flow field is assumed to be incompressible, with constant thermo-physical properties following the ideal gas equation of state, evaluated at ambient condition. The discretization in space and time is second-order accurate and performed relying upon the guidelines described in [20, 18, 21, 19], which report full details on the physical models, the required space-time resolution, and the experimental validation. In this section, however, we briefly recall the most relevant aspects of the CFD model, for the sake of completeness. From the point of view of the space discretization, the domain extension must be suitably chosen to avoid possible non physical numerical phenomena, such as spurious reflections at the boundaries and alteration

to the pressure field. Finally, the domain extension has to directly set a good trade-off in between the achievement of reliable flow field resolution and the available computing resources. The 2D simulation domain was extended up to 4.5 (equatorial) rotor diameters upstream the axis of rotation, 12 diameters on both lateral sides, and 3 diameters downstream. Instead the 3D simulations employed a domain whose lateral boundaries were placed at 3 diameters only from the axis, by virtue of the overall lower blockage effect in the 3D simulation with respect to the 2D one, as shown and discussed in detail in [20] for H-shape rotors and in [19] for troposkein ones. In spanwise direction the 3D domain boundary was set up to twice the height of the half turbine model. The domain was then partitioned into non overlapping polyhedral elements suitably clustered near solid walls to fulfill the $y^+ < 1$ requirement. The computational domains have been built following the clustering guidelines provided in [19], featuring a minimum spacing normal off solid wall equal to $2 \cdot 10^{-4}$ times the blade chord, in agreement to fulfillment of the well know constraint on $y^+ \approx 1$; a local growing factor of the boundary layer was selected equal to 1.2. See Figure 1 displays on the RHS a detail of the adopted grid. Preliminary computations have been led focusing on the power coefficient value and fixing a threshold level of acceptable accuracy. The relative reduction in between solutions obtained on subsequent refined meshes were assumed to be satisfactory when the relative error computed on C_P was lower than 2%. The "sensitivity-converged" 2D mesh adopted in this study consists of 120000 cells while the 3D grid used for the Troposkein rotors TW and DW composed by nearly 20 millions of polygonal cells.

A backward differentiation formula BDF2 was employed for the time discretization, using 720 time-steps per revolution. Computations have been run till a periodic solution was achieved at each operating case selected (15 to 20 turbine revolutions were required to get achieve the periodic solution).

The turbulence modeling approach adopted was based on the Boussinesq hypothesis and the model selection was mainly driven by the results presented in [19], where, the comparison of measured and predicted performance values highlighted that the low-Reynolds version of the $k - \omega$ SST model seems properly suited for predicting the turbine flow field and performance, especially at high tip speed ratio operation. In order to draw attention to the aerodynamic phenomena, we performed a complete 2D numerical campaign and then considered 3D test cases at relevant operating conditions near peak-power production and at higher TSR values.

The boundary conditions at the inlet prescribe the freestream velocity, the turbulence intensity level and the turbulent viscosity ratio, *i.e.* a 1 % turbulence intensity (the experimental value) and a viscosity ratio ν_T/ν equal to one, which is a typical value adopted with this turbulence model. The wind turbine is rotating at a constant regime equal to 300 rpm, and the operating conditions studied are defined by modifying the wind freestream velocity, according to selected TSR values. Instead, at the outlet boundary, the static pressure is imposed and in presence of backflow condition, the fluid is entrained at ambient total pressure and temperature, low turbulence level. At solid wall the dissipation rate is imposed using the wall boundary condition.

4 Wind turbine rotors: CFD performance prediction

This section presents the results of the thorough numerical investigation focused on the behaviour of different rotor configurations and blade shape. The full operating ranges (in terms of TSR conditions) are taken into account, from near start-up toward high load condition. Please notice that previous investigations led by the same authors already highlighted rather good agreement with reference measurements performed by one of the authors. Therefore, in this

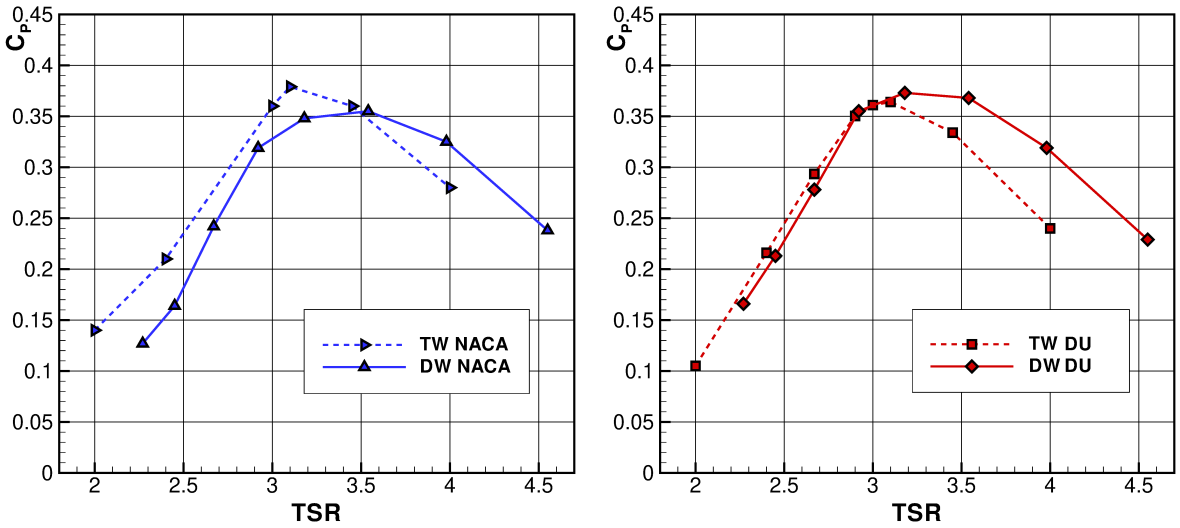

Figure 2: TW & DW, 2D power coefficient as a function of the TSR number using NACA/DU airfoil profiles (left/right)

part of the work, for the sake of the figures clarity, the experimental results are not reported.

Figure 2 shows the performance curves for different Troposkein design, considering the two selected airfoil sections, applied to each machine. The left frame of Figure 2 shows a comparison between the two rotors adopting the NACA0021 profile in their blades; the TW rotor is characterized by a higher maximum C_P value, that is obtained at a lower TSR value than the latter configuration. Instead, the DW rotor exhibits a more regular behaviour near peak power condition, characterized by a large plateau around peak C_P condition. When the two rotor architectures are considered with the same DU profile, see the right frame of Figure 2, the plateau region characterizing the DW model is still present with respect to the TW one, but in this case the DW outperforms TW in terms of peak C_P. Therefore, at fixed airfoil profile, the solidity effect is the relevant issue that modifies the flow field and 'moves' the C_P curve towards lower TSR values, as also shown in [14]. The results also suggest that the rotor DW with its solidity ensures better performance at high TSR operating conditions; at the same time, as shown in the left frame of Figure 3, the use of a DU profile, designed to better deal with the complex vortical structures developing in the downwind region, can improve the performance at low TSR condition.

In the following, the aerodynamic performance of selected rotors are discussed both at full TSR operating range and in detail at peak power condition.

4.1 Wind Rotors designed with different blade profiles

The DU profile has been realized to improve the machine performance at low TSR operating conditions where the flow field becomes intrinsically more complex from the aerodynamic point of view, as large separation regions occur and large-scale vortices travel along the profiles and are convected downstream. It can be readily observed from Figure 3 how the DU profile endows the DW rotor of higher power exchange capability. The right frame of Figure 3, displays the drag and lift coefficients (based on relative flow velocity of the flow upstream of each profile) for the DW NACA (TSR=3.54) and the DW DU (TSR=3.18) at their respective peak C_P condition, computed neglecting the induction effect. Despite a direct comparison is challenging due to

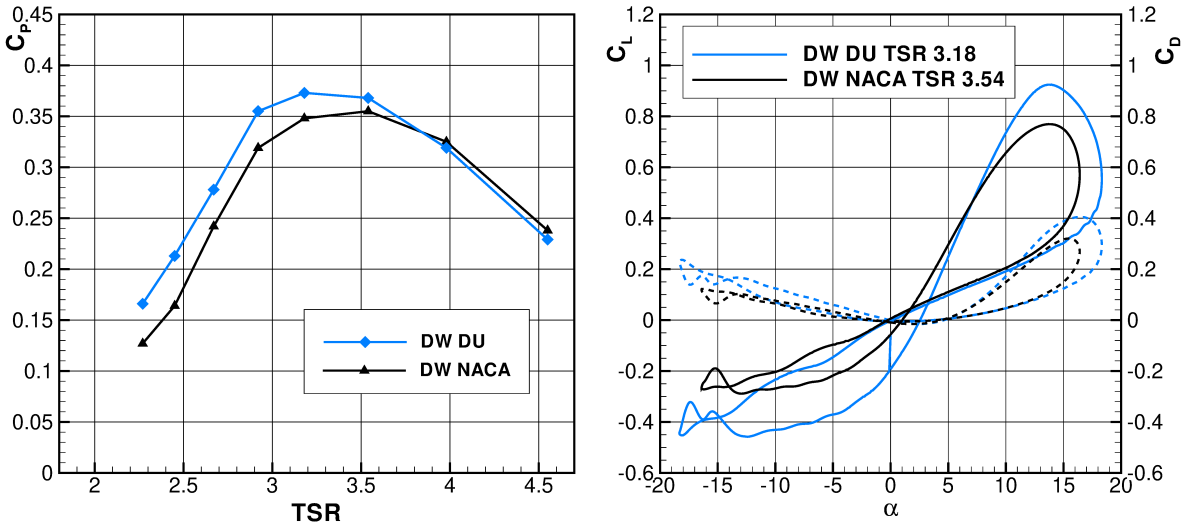

Figure 3: DW using DU/NACA airfoils: 2D power coefficient as a function of the TSR number (left); lift and drag coefficient as a function of local angle of attack α at peak power operating point

the variations both of angle of attack and unsteadiness, the DU-based machine clearly shows a higher aerodynamic efficiency level, especially for the increased lift coefficients values with respect to the NACA-based machine. Further insights into the local flow field development can be achieved from Figure 4, which displays the evolution of the momentum coefficient of a single blade during the whole rotor revolution, along with the visualization of the non dimensional velocity contours at selected blade angular positions. Higher torque values are provided, by the DU profile, both in the upwind and downwind regions, as displayed for instance by the flow field at $\vartheta = 240°$. The velocity field past the NACA0021 and past DU profile are, in fact, rather similar at point $\vartheta = 90°$, and the two fields still provide the same aerodynamic performance; the same applies also to the solutions at $\vartheta = 120°$, even though in this case, the DU profile detaches larger scale vortices. Finally when moving in the leeward part of the downwind region, the DU capability of better deal with the onset of transition, and separation from solid wall, becomes relevant. This result indicate that, even though the larger contribution to C_P value comes from the upwind region, the downwind operational behaviour is of great importance for the rotor aerodynamics, and the shape of the profile can have a crucial role in this part of the rotation.

Figure 5 displays a summary of the results of the 2D computations performed on the TW turbine. This rotor highlights indeed a different behaviour, *i.e.* from peak power condition, towards the highest load at TSR=4, the torque coefficient is increased when operating using the symmetrical NACA profile. The increased rotor solidity with respect to the previous rotor design improves the aerodynamic behavior at large TSR values. The DU profile, however, still demonstrates its potential in dealing with the most complex operation in the downwind region of the rotation, providing higher local torque contribution.

To finally gather all the numerical tests, Figure 6 collect the C_P curves for all the considered configurations and also presents, in dimensional form, the power harvested by the rotors against the freestream wind velocity. In this figure, the actual capability, also retaining the overall efficiency, is displayed, showing for example that the coupling between the DU profile with the DW rotor guarantees the best performance over most of the operating range, while the use of

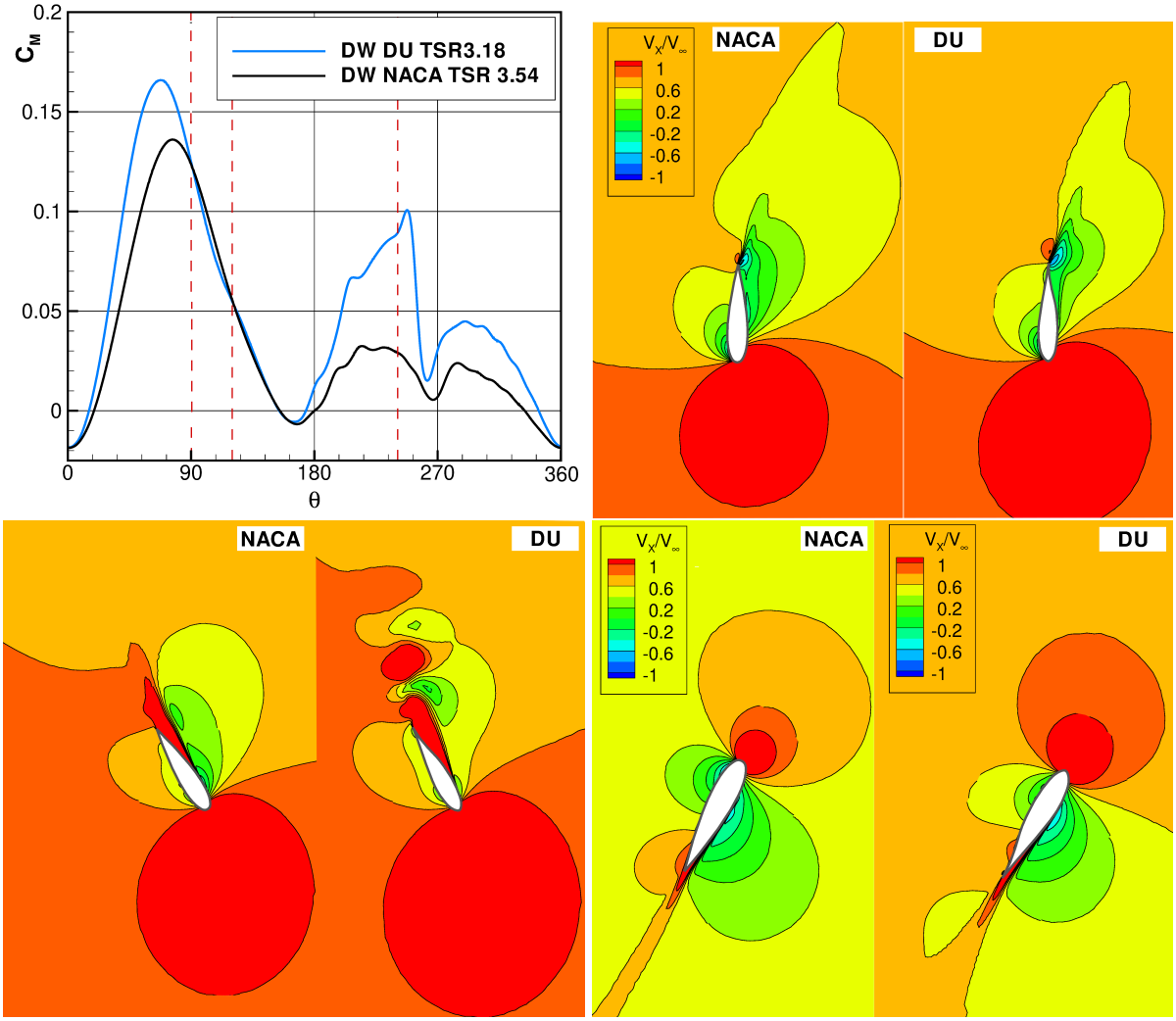

Figure 4: DW: torque coefficient computed at peak power operating point, TSR=3.18; 3.54 using a DU; NACA airfoil profile. Non dimensional streamwise velocity at azimuthal position $\vartheta = 90°$ (top right), $\vartheta = 120°, 240°$ (bottom left,right)

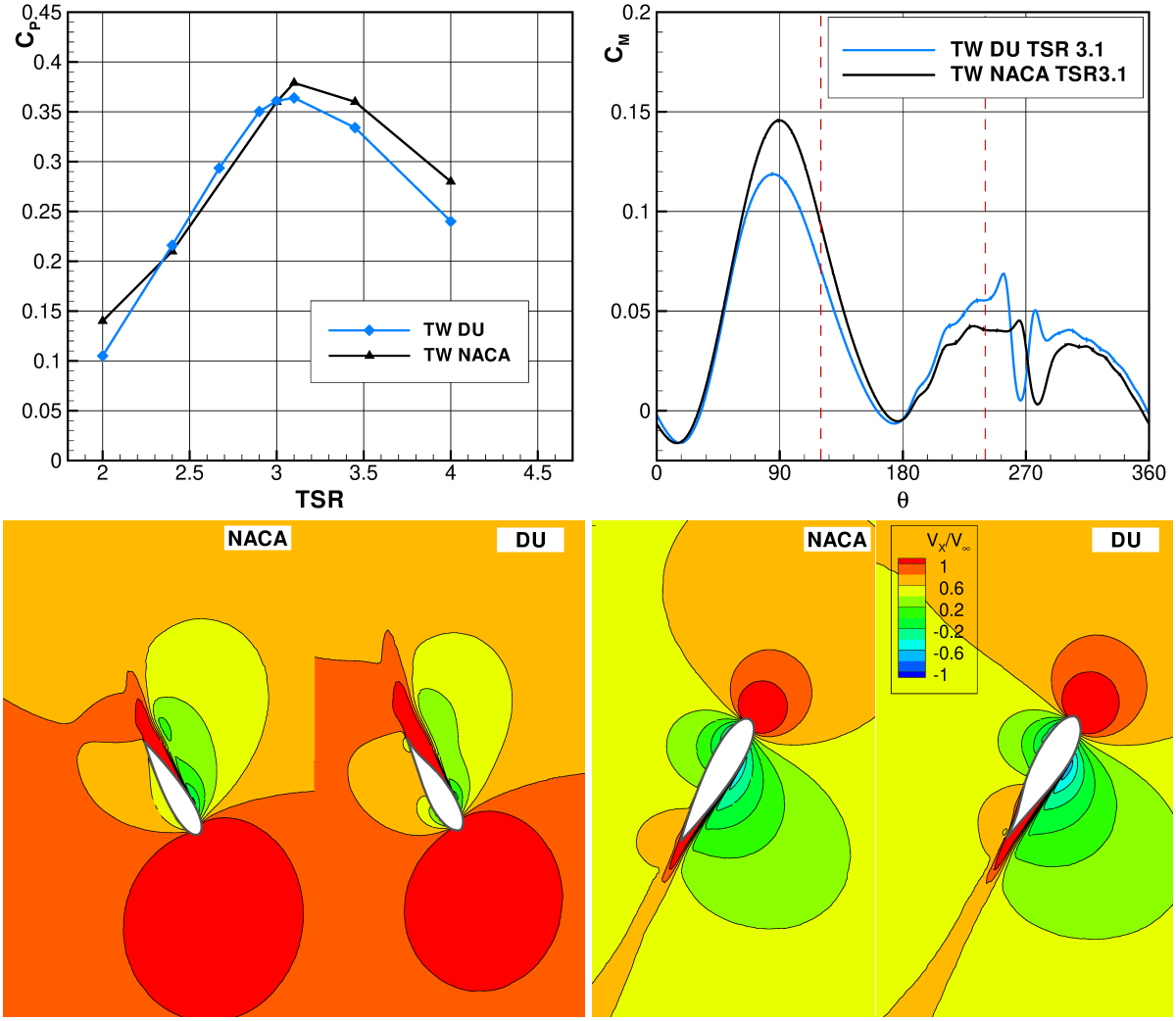

Figure 5: TW: 2D power coefficient as a function of the TSR number using NACA/DU airfoil profiles and moment coefficient at peak power condition (top); non dimensional streamwise velocity at azimuthal position $\vartheta = 120°, 240°$ (bottom)

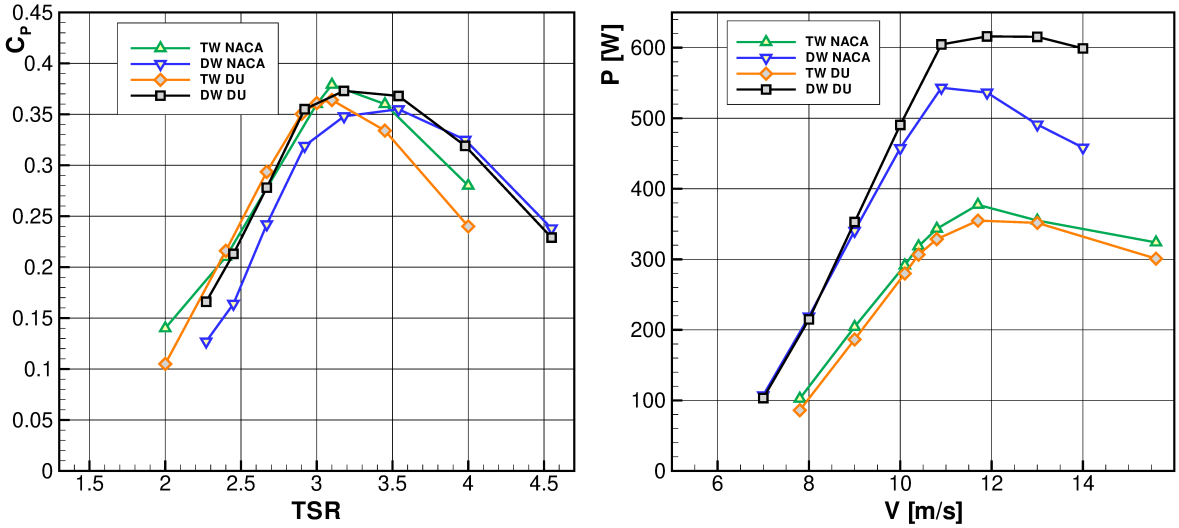

Figure 6: 2D VAWTs: power coefficient as a function of the TSR number for the selected wind turbines (left); Power as a function of the freestream velocity (right)

the NACA with the DW rotor penalizes significantly the power harvesting capability at high tip speed ratio. However, those levels must be considered just as rough indications of the turbine performance, and used also in comparative way, since 3D effects play a key role in the final definition of each configuration, as discussed in the following section.

5 3D aerodynamic study of Troposkein VAWTs near peak power condition

The effects of the fully 3D troposkein rotor shape is considered in this section for the sake of a wider cross comparison between the different rotors and airfoil sections, considering the different solidity values, machine aspect ratio, and Reynolds number. The 3D behaviour of a wind turbine of troposkein kind presents complex fluid dynamic flow structures developing along the turbine span, alternative than those occurring, for example, in a H-shaped one, which can roughly be seen as an extension of the midspan section with parasitic drag effects related to the spokes and the blade tips. In this paragraph, the 3D results of selected troposkein configurations are presented to investigate their aerodynamic performance; table 2 lists the 3D test cases presented.

Rotor	Airfoil	TSR	$C_{P,num}$
TW	NACA	3.15	0.276
DW	DU	3.54	0.283
DW	NACA	3.54	0.277

Table 2: 3D TW & DW test cases considered near peak power condition

Figure 7 shows the torque harvesting capability of the DW VAWT at TSR=3.54 using both the NACA and DU airfoils, in comparison to 2D values. At first, it is to be noted that the DW-DU configuration is here considered for a TSR higher than its optimal one, while the DW-NACA is in optimal condition. Despite this, the torque coefficient over the full revolution obtained with the DU profile still outperforms the rotor with the NACA profile, especially in

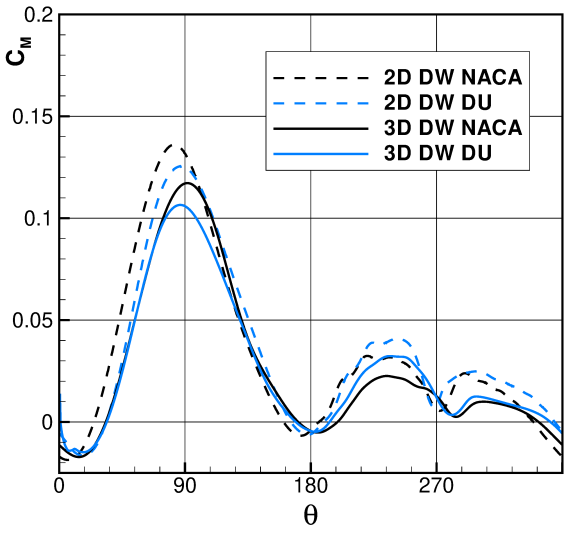

Figure 7: DW rotor using NACA and DU profiles at TSR_{eq}=3.54: 2D and 3D C_M values as a function of the azimuthal position

the leeward section of the downwind blade motion. This has been already found for the 2D simulation and remains valid for the 3D simulation, as also reported by table 2. This overall result can be better appreciated by considering the spanwise evolution of torque coefficient along the span reported in Figure 8. While a slightly lower peak in torque coefficient features the DW-DU configuration, this configuration systematically outperforms the DW-NACA rotor in the downwind region, where the blade operates in a complex vortical flow. This feature, previously commented for the 2D-equatorial section, still holds in the sections closer to the tip, where large separations take place and the complexity of the flow increases, due to the low local TSR. The selection of the blade profile offers, therefore, not-trivial advantages also in flow conditions where dynamic stall and vortex interaction take place. Moreover, the present results indicate that a selection based on the 2D equatorial section can be extended to the full 3D shape of the machine, despite the complexity of troposkein configuration.

A further interesting comparison can be made modifying the rotor configuration while using the same NACA profile. In this case, the two rotors were simulated at their respective peak C_P conditions, namely TSR = 3.1 for the TW turbine and TSR = 3.54 for the DW one. Interestingly, for these conditions the two machines provide exactly the same value of C_P, while in the 2D simulations the TW rotor was providing a slightly higher peak power coefficient, as also clearly visible by comparing the 2D trends in the left frame of Figure 9. The situation changes in 3D, where differences between the two rotor performance appear well defined; the DW rotor outperforms the TW one in the upwind phase of the revolution, in particular in the leeward region, while the TW outperforms the DW in the downwind part. These two effects counterbalance themselves, leading to similar overall performance. The two rotor differ by the values of solidity, lower for DW, and Reynolds number, higher for DW. The increased Reynolds number contributes to explain the improved performance of the DW turbine in the upwind-leeward region: in this part of the revolution the highest angle of attack is reached, which leads to the peak of C_M, followed by a separation and the subsequent drop in performance; an increased Reynolds number can slightly delay the separation, guaranteeing higher aerodynamic performance. The low solidity of DW rotor can, instead, explain the lower performance in this rotor

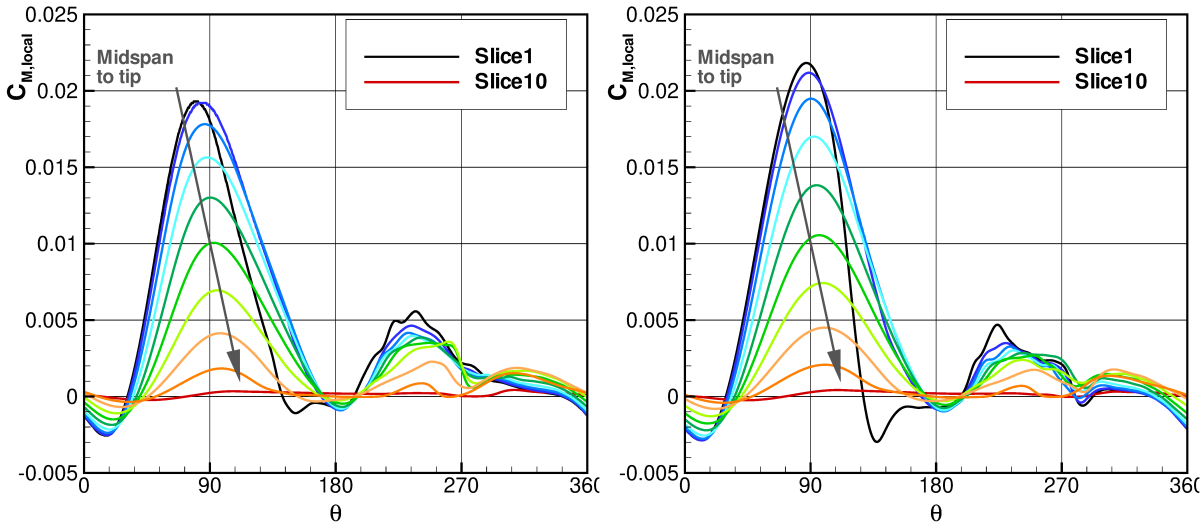

Figure 8: DW using DU/NACA profile (left/right) at TSR_{eq}=3.54: Moment coefficient as a function of azimuthal angle for 3D computations at selected spanwise positions

in the downwind phase of the revolution: as a consequence of the lower solidity, the peak C_P condition moves towards higher TSR values, which leads to lower angle of attack and, hence, lower lift coefficients generated by the blades. These features holds all along the rotor span, as visible by comparing the trends shown in the right frame of Figure 8 with the right frame of Figure 9.

6 Conclusions

This paper has presented a computational comparative analysis of several vertical axis wind turbines, with the aim of studying the impact of blade profile and rotor architecture on the capability of the wind turbine to extract power from the wind. Two rotors and two blade profiles have been selected, leading to four configurations featuring different solidity and equatorial Reynolds number; two of these configurations were characterized experimentally in wind tunnel experiments and were used, in previous works, to construct and validate the computational flow models used here.

Focusing on the equatorial section of the rotor, the comparison shows that the use of non-symmetric laminar profiles, such as the DU considered here, can lead to very significant advantages in complex regions of the flow, such as in the downwind phase of the revolution, where the blade undergoes high oscillations of angle of attack and interact with viscous/vortical structures detached by adjacent blades. Indeed, the troposkein rotor is highly 3D, but the machine performance and power exchange process are dominated by the flow features in the equatorial region, where the highest TSR and flow rate occur.

When considering the fully 3D configurations of the rotor, the positive effect of using the non-symmetric profile is confirmed also along the span, especially because the tip regions of the rotor exhibits even larger separated regions, with respect to the equatorial section, due to the local low tip speed ratio. A relevant effect of the rotor solidity was also observed, as the different design relying upon the same airfoil exhibited the same performance at different TSR, confirming the 2D results; this suggests that a solidity formulation only based on the equatorial section can be considered representative for the whole troposkein rotor. Reynolds number ef-

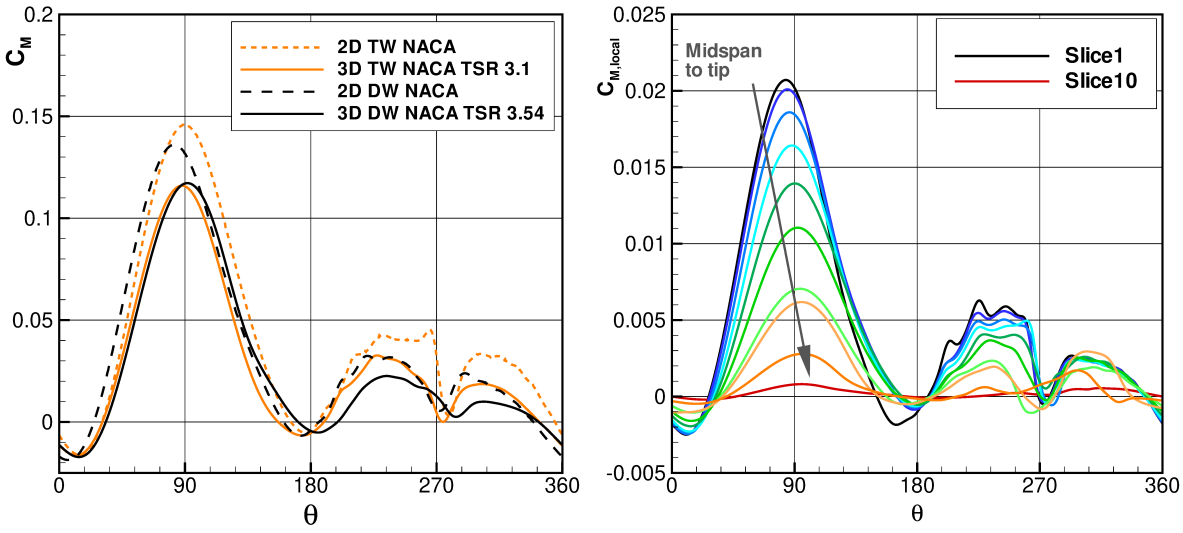

Figure 9: TW & DW using NACA profile: Moment coefficient as a function of azimuthal angle (left); TW using NACA profile at TSR_{eq}=3.1: Moment coefficient as a function of azimuthal angle for 3D computations at selected spanwise positions (right)

fects were also observed by analyzing the local behaviour of the blades, especially in the phase of leeward blade motion, where higher Reynolds can delay the onset of blade separation.

This study clearly indicates that detailed aerodynamic features can play a significant role in determining the capability of such machines to harvest power, owing to the complexity of VAWT aerodynamics. Such findings prompt to perform further investigations oriented towards the optimization of this class of rotors, not only in their peak power condition, but across their entire application range.

References

[1] StarCCM+, release 19, https://www.plm.automation.siemens.com/global/en/products/.

[2] F. Balduzzi, A. Bianchini, G. Ferrara, and L. Ferrari. Dimensionless numbers for the assessment of mesh and timestep requirements in CFD simulations of Darrieus wind turbines. *Energy*, 97:246–261, 2016.

[3] F. Balduzzi, A. Bianchini, R. Maleci, G. Ferrara, and L. Ferrari. Critical issues in the CFD simulations of Darrieus wind turbines. *Energy*, 85:419–435, 2016.

[4] F. Balduzzi, J. Drofelnik, A. Bianchini, G. Ferrara, L. Ferrari, and M.S. Campobasso. Darrieus wind turbine blade unsteady aerodynamics:a three-dimensional Navier-Stokes CFD assessment. *Energy*, 128:550–563, 2017.

[5] G. Banga, A. Dessoky, T. Lutz, and E. Kramer. Improved double-multiple-streamtube approach for h-darrieus vertical axis wind turbine computations. *Energy*, 90:439–451, 2009.

[6] L. Battisti, E. Benini, A. Brighenti, S. Dell'Anna, M. Raciti Castelli, V. Dossena, G. Persico, U.S. Paulsen, and T.F. Pedersen. Wind Tunnel Testing of the DeepWind Demonstrator in Design and Tilted Operating Conditions. *Energy*, 111:484–497, 2016.

[7] L. Battisti, G. Persico, V. Dossena, B. Paradiso, M.R. Castelli, A. Brighenti, and E. Benini. Experimental benchmark data for h-shaped and troposkien VAWT architectures. *Renewable Energy*, 125:425–444, 2018.

[8] A. Bianchini, F. Balduzzi, G. Ferrara, G. Persico, V. Dossena, and L. Ferrari. A Critical Analysis on Low-Order Simulation Models for Darrieus VAWTs: How Much Do They Pertain to the Real Flow? *Journal of Engineering for Gas Turbines and Power*, 2019.

[9] M. Borg, K. Wang, M. Collu, and T. Moan. A Comparison of Two Coupled Model of Dynamics for Offshore Floating Vertical Axis Wind Turbines (VAWT). volume -, Oct. 2014.

[10] L. Chao, Z. Sonye, X. You-Lin, and X. Yiqing. 2.5D large eddy simulation of vertical axis wind turbine in consideration of high angle of attack. *Renewable energy*, 51:317–330, 2013.

[11] P. Chatelain, M. Duponcheel, D.G. Caprace, Y. Marichal, G. Winckelmans S. Shamsoddin, and F. Porté-Agel. Vortex particle-mesh simulations of vertical axis wind turbine flows: from the blade aerodynamics to the very far wake. *Journal of Physics*, 753:317–328, 2017.

[12] M. Claessens. *The Design and Testing of Airfoils in Small Vertical Axis Wind Turbines*. PhD thesis, Delft University of Technology, Delft, the Nederlands, 01 2006.

[13] G. J. M. DARRIEUS. Turbine having its rotating shaft transwerse to the flow of the current, US patent 1,835,018, Dec. 8, 1931.

[14] PL. Delafin, T. Nishino, L. Wang, and A. Kolios. Effect of the number of blades and solidity on the performance of a vertical axis wind turbine. *Journal of Physics: Conference Series*, 1742:022033, 2026.

[15] V. Dossena, G. Persico, B. Paradiso, L. Battisti, S. Dell'Anna, E. Benini, and A. Brighenti. An Experimental Study of the Aerodynamics and Performance of a Vertical Axis Wind Turbine in a Confined and Unconfined Environment. *ASME Journal of Energy Resources Technology*, 137(051207), Sept. 2015.

[16] M. Elkhoury, T. Kiwata, and E. Aoun. Experimental and numerical investigation of a three-dimensional vertical-axis wind turbine with variable-pitch. *J. Wind Eng. Ind. Aerodyn*, 139:111–123, 2015.

[17] Carlos Simao Ferreira. *The near wake of the VAWT, 2D and 3D views of the VAWT aerodynamics*. PhD thesis, Delft University of Technology, Delft, the Nederlands, 2009.

[18] N. Franchina, O. Kouaissah, G. Persico, and M. Savini. Three-dimensional CFD simulation and experimental assessment of the performance of a H-shaped vertical axis wind turbine at design and off-design conditions. *Int. J. Turbomach. Propuls. Power*, 4(3),30, 2019.

[19] N. Franchina, O. Kouaissah, G. Persico, and M. Savini. Three-dimensional modeling and investigation of the flow around a troposkein vertical axis wind turbine at different operating conditions. *Renewable Energy*, 199:368–381, 2022.

[20] N. Franchina, G. Persico, and M. Savini. 2D-3D computations of a vertical axis wind turbine flow field: modeling issues and physical interpretations. *Renewable Energy*, 136:1170–1189, 2019.

[21] N. Franchina, G. Persico, and M. Savini. Three-dimensional unsteady aerodynamics of a H-shaped vertical axis wind turbine over the full operating range. *Journal of Wind Engineering & Industrial Aerodynamics*, 206, 2020.

[22] N. Fujisawa and S. Shibuya. Observations of dynamic stall on Darrieus wind turbine blades. *Wind engineering and industrial aerodynamics*, 89:201–214, 2001.

[23] Q. Li, T. Maeda, Y. Kamada, J. Murata, M. Yamamoto, T. Ogasawara, K. Shizimu, and T. Kogaki. Study on power performance for a straight-bladed vertical axis wind turbine by field and wind tunnel test. *Renewable Energy*, 90:291–300, 2016.

[24] M.A. Miller, S. Duvvuri, W.D. Kelly, and M. Hultmark. Rotor solidity effects on the performance of vertical-axis wind turbines at high Reynolds numbers. *Journal of Physics: Conference Series*, 1618:052015, sep 2018.

[25] A. Orlandi, M. Collu, S. Zanforlin, and A. Shires. 3D URANS analysis of a vertical axis wind turbine in skewed flows. *Journal of Wind Engineering and Industrial Aerodynamics*, 147:77–84, 2015.

[26] U.S. Paulsen, M. Borg, H.A. Madsen, T.F Pedersen, J. Hattel, E. Ritchie, C.S. Ferreira, H. Svendsen, P.A. Berthelsen, and C. Smadja. Outcomes of the DeepWind conceptual design. *Energy Procedia*, 80:329–341, 2015.

[27] U.S. Paulsen, H.A. Madsen, J.H. Hattelc, I. Baranc, and P.H. Nielsen. Design optimization of a 5 mw floating offshore vertical-axis wind turbine. *Energy Procedia*, 35:22–32, 2013.

[28] A. Rezaeiha, I. Kalkamn, and B. Blocken. CFD simulation of a vertical axis wind turbine operating at a moderate tip speed ratio: guidelines for minimum domain size and azimuthal increment. *Renewable Energy*, 107:373–385, 2017.

[29] A. Rezaeiha, I. Kalkmanb, H. Montazeria, and B. Blocken. Effect of the shaft on the aerodynamic performance of urban vertical axis wind turbines. *Energy conversion and management*, 149:616–630, 2017.

[30] S.-C. Roh1 and S.-H. Kang. Effects of a blade profile, the reynolds number, and the solidity on the performance of a straight bladed vertical axis wind turbine. *Journal of Mechanical Science and Technology*, 27(299-3307), 2013.

[31] A. Rossetti and G. Pavesi. Comparison of different numerical approaches to the study of the H-Darrieus turbines start-up. *Renewable energy*, 50:7–19, 2017.

[32] S. Shamsoddin and F. Porté-Agel. Large eddy simulation of vertical axis wind turbine wakes. *Energies*, 7:890–912, 2014.

[33] M.S. Siddiqui, A. Rasheedb, T. Kvamsdala, and M. Tabib. Effect of turbulence intensity on the performance of an offshore vertical axis wind turbine. *Energy Procedia*, 80:312–320, 2015.

[34] G. Tescione, D. Ragni, He C, S. Ferreira, and G.J.W. van Bussel. Near wake flow analysis of a vertical axis wind turbine by stereoscopic particle image velocimetry. *Renewable Energy*, 70:47–61, 2014.

[35] M. R. Tirandaz and A. Rezaeiha. Ceffect of airfoil shape on power performance of vertical axis wind turbines in dynamic stall: Symmetric airfoil. *Renewable Energy*, 173:422–441, 2021.

[36] Luca Vita, Uwe Schmidt Paulsen, Troels Friis Pedersen, Helge Aagaard Madsen, and Flemming Rasmussen. Deep wind: A novel floating wind turbine concept. *Windtech International*, 6(4):29–31, 2010.